

The NLO electroweak effects on the Higgs production in association with bottom quark pair at the LHC

Yu Zhang^{1,2,*}

¹*School of Physics, Nanjing University, Nanjing, Jiangsu, 210093, China*

²*CAS Center for Excellence in Particle Physics, Beijing 100049, China*

Abstract

The dominant contribution to the Higgs production in association with bottom quark pair at the LHC is gluon-gluon fusion parton subprocess. We present a complete calculation of the next-to-leading order (NLO) electroweak (EW) corrections to this channel. The other small contributions with quarks in the initial state are calculated at tree level. We find that the NLO EW corrections can suppress the leading order (LO) contributions significantly.

PACS numbers:

*Electronic address: dayu@nju.edu.cn

I. INTRODUCTION

The discovery of the long waited Higgs boson at the LHC by ATLAS[1] and CMS[2] in July 2012 is a milestone in the particle physics. After this achievement, more precise examination of this new boson's properties becomes one of the most important endeavors for the LHC and future colliders. The recent analyses show that its couplings are compatible with those predicted by the Standard Model(SM)[3, 4]. However, the interpretation of Beyond the Standard Model(BSM) scenarios is still an open issue and more precise predictions for this particle are urgently required.

The production of a Higgs boson in association with bottom quarks at hadron colliders has been extensively studied in the literature. Depending on the choice of the flavour-scheme in the partonic description of the initial state and on the identified final state, one can consider a number of different partonic sub-processes for associated bottom-Higgs production: while the choice of the 4 versus 5 flavour scheme is mainly theoretically motivated, resulting in a reordering of the perturbative expansion [5], the requirement of a minimum number of tagged b in the final state is physically relevant in the signal extraction. There are mainly three different types of production processes: i) the inclusive one, where no bottom quark jet is tagged, dominated by the bottom quark fusion process $b\bar{b} \rightarrow H$, ii) the semi-inclusive one, where only one bottom quark is tagged, dominated by process $bg \rightarrow bH$, iii) the exclusive one where both bottom jets are tagged, almost entirely dominated by $gg \rightarrow b\bar{b}H$, with only a small contribution from $q\bar{q} \rightarrow b\bar{b}H$.

The analysis of the relative weights of the above three different types of production processes are present in [6, 7], where also the $b\bar{b} \rightarrow H$ process is computed at next-to-leading order (NLO) in QCD. Besides, the $b\bar{b} \rightarrow H$ process has been calculated at next-next-to-leading order (NNLO) in QCD [8] while the electroweak NLO corrections have been presented in [9]. For the associated semi-inclusive production process $bg \rightarrow bH$, NLO QCD corrections can be obtained from [10–12], and purely-weak and EW corrections have been presented in [13, 14] respectively. Finally, for the exclusive process, where two bottom jets are tagged in the final state, the cross section is known through NLO QCD in the SM in the four-flavor scheme (4FS) [15–17] and matched to parton showers in [18].

This paper is strongly motivated by the possible relevance of the associated bottom-Higgs production in the experimental examination of the bottom-quark Yukawa couplings at the LHC. The purpose of this paper is to provide and study the EW corrections to the fully exclusive process $pp \rightarrow b\bar{b}h$ in the 4FS, where the final state includes two high transverse momentum bottom quarks, for the first time. The rest of this paper is organized as follows: in section II, we describe the

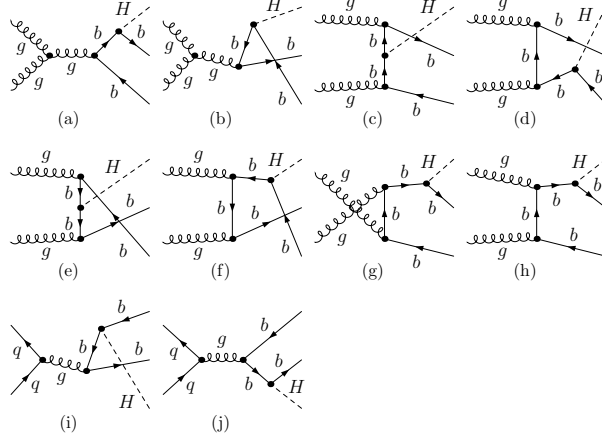


FIG. 1: The Feynman diagrams at tree level.

structure of EW NLO calculation for the $b\bar{b}H$ production at the LHC. The numerical results are presented and discussed in section III. Finally a summary is given.

II. STRUCTURE OF THE CALCULATION

A. Leading order consideration

For the process $pp \rightarrow b\bar{b}H + X$, at tree level the main partonic subprocesses are $gg \rightarrow b\bar{b}H$ and $q\bar{q} \rightarrow b\bar{b}H$ (q stands for light quark). The corresponding Feynman diagrams are displayed in the first two lines (a-h) and the last line (i-j) of Fig.1, respectively. The dominant contributions arise from gg of order $\mathcal{O}(\alpha_s^2\alpha)$, and the $q\bar{q}$ contributions of the same order are much smaller since they involve only the s channel diagrams, which are obviously suppressed at high energy, and the corresponding parton density is much smaller than that of gluon at the LHC. It is noticed that there are also contributions of the order $\mathcal{O}(\alpha^3)$ from the tree-level EW Feynman diagrams of $q\bar{q}$ annihilations, are neglected in our calculation since they are extremely small.

At LO ($\mathcal{O}(\alpha_s^2\alpha)$), the total cross section for $pp \rightarrow b\bar{b}H + X$ can be written as

$$\sigma_{LO}^{pp} = \sum_{ij} \frac{1}{1 + \delta_{ij}} \int dx_1 dx_2 \left[\mathcal{F}_i^p(x_1, \mu_F) \mathcal{F}_j^p(x_2, \mu_F) \hat{\sigma}_{LO}^{ij}(x_1, x_2, \mu_R) + (x_1 \leftrightarrow x_2) \right], \quad (1)$$

where (i, j) denotes (g, g) (q, \bar{q}), $\hat{\sigma}_{LO}^{ij}$ the corresponding partonic cross section at LO and $\mathcal{F}_j^p(x, \mu_F)$ represents the distribution function at the scale μ_F of parton i (i.e., quark or gluon) at momentum fraction of x .

B. NLO EW contribution to $gg \rightarrow b\bar{b}H$ production

In the following, we discuss the NLO EW contributions to the $gg \rightarrow b\bar{b}H$ production. These contributions are of order $\mathcal{O}(\alpha_s^2\alpha^2)$. The contributions at the same order from the suppressed $q\bar{q}$ annihilations are much smaller and will be neglected.

The NLO EW correction includes both the virtual and real photon contribution. The virtual corrections are induced by the self-energies, triangle (3-point), box (4-point), and pentagon (5-point) diagrams, and contain ultraviolet(UV) divergences and infrared (IR) soft divergences. First, we discuss the issue of renormalization which guarantees the result ultraviolet safe. It should be noted that the box and pentagon diagrams are both UV finite. To cancel the UV divergences, the renormalization of the bottom quark mass, the Higgs mass, the electric coupling, the bottom Yukawa coupling, and the external wave functions are required. The relevant wave functions and masses are renormalized by taking the on-mass-shell renormalization scheme. The renormalization constants can be found in Ref.[19]. To specify the fine structure constant, we adopt the G_μ scheme with $\alpha_{G_\mu} = \frac{\sqrt{2}M_W^2 G_\mu}{\pi} (1 - \frac{M_W^2}{M_Z^2})$ as an input parameter. With this choice, the EW corrections are independent of logarithms of the light fermion masses, and the calculation is consistently done by modifying the renormalization constant according to

$$\delta Z_e^{G_\mu} = -\frac{1}{2}\delta Z_{AA} - \frac{s_W}{2c_W}\delta Z_{ZA} - \frac{1}{2}\Delta r^{(1)}, \quad (2)$$

where the explicit expressions of $\Delta r^{(1)}$ are detailed in Ref.[19]. Concerning to bottom quark, the pole mass enters the kinematic variables of the matrix element and the phase space, and a running bottom mass is usually used in the improved Higgs Yukawa coupling. For NLO QCD calculations, the two masses can be treated as different variables. However, as the bottom mass is of EW origin, this treatment is not feasible for NLO EW analysis. Such treatment would violate Ward identities involving m_b [20], and the cancellation of UV poles will be incomplete. Consequently, one has to implement a common value, either the pole mass or the running mass, for the bottom quark mass that enters the kinematic variables of the matrix element, the phase space and the variable of Higgs-bottom Yukawa couplings[21]. In our calculation, the cancellation of UV poles are checked by using the bottom pole mass as a common value.

Eliminating the UV divergences, the virtual corrections still involve soft IR divergences. In our consideration, to obtain an IR safe result, we need to take into account the real photon emission contributions arise from the subprocess:

$$g + g \rightarrow b + \bar{b} + H + \gamma, \quad (3)$$

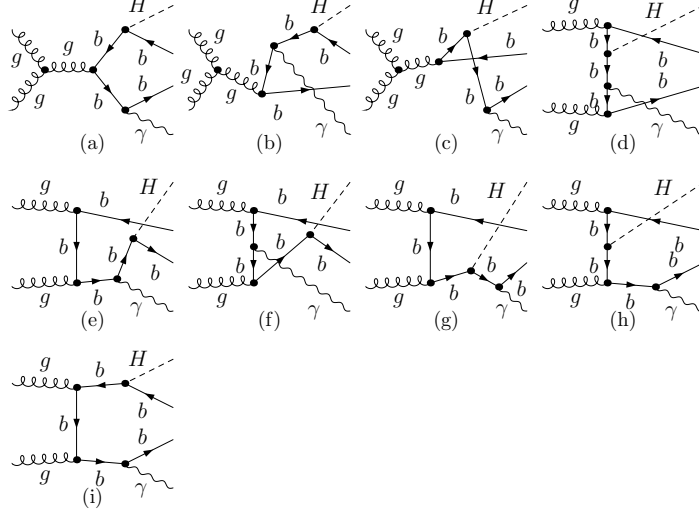


FIG. 2: The representative Feynman diagrams for the real photon emission process $gg \rightarrow b\bar{b}H + \gamma$.

of which the representative Feynman diagrams are shown in Fig.2. The photon induced IR singularities originating from the virtual corrections can be extracted and cancelled exactly with those in the real photon emission corrections. This cancellation can be realized either by the two cutoff phase space slicing method [22] or the dipole subtraction method [23–25]. In this work, we adopt the two cutoff phase space slicing method with $\delta_s = 1 \times 10^{-5}$ and verified the result is consistence with the result by using dipole subtraction.

Since the invariant mass of the bottom pair can equal to Higgs or Z boson mass, the intermediate Higgs or Z boson can be on-shell, which is illustrated in Fig.3. The interference between the corresponding diagrams and the LO diagrams would contain a resonant propagator $\frac{1}{M_{b\bar{b}}^2 - M_{(H/Z)}^2}$, which leads to singularities in the vicinity of $M_{b\bar{b}}^2 \sim M_{(H/Z)}^2$. We regulate the singularities by making the replacement of $\frac{1}{M_{b\bar{b}}^2 - M_{(H/Z)}^2} \rightarrow \frac{1}{M_{b\bar{b}}^2 - M_{(H/Z)}^2 + iM_{(H/Z)}\Gamma_{(H/Z)}}$. The corresponding contribution is found to be negligible in the total NLO EW cross section, but it is important for several differential kinematic distributions.

We apply the FeynArts-3.7 package [26] to generate the Feynman diagrams automatically and the corresponding amplitudes are algebraically simplified by the FormCalc-7.2 program [27]. In the calculation of one-loop Feynman amplitudes, the LOOPTOOLS-2.8 package [27] is adopted for the numerical calculations of the scalar and tensor integrals, in which the n -point ($n \leq 4$) tensor integrals are reduced to scalar integrals recursively by Passarino-Veltman algorithm and the 5-point integrals are decomposed into 4-point integrals by the method of Denner and Dittmaier [28].

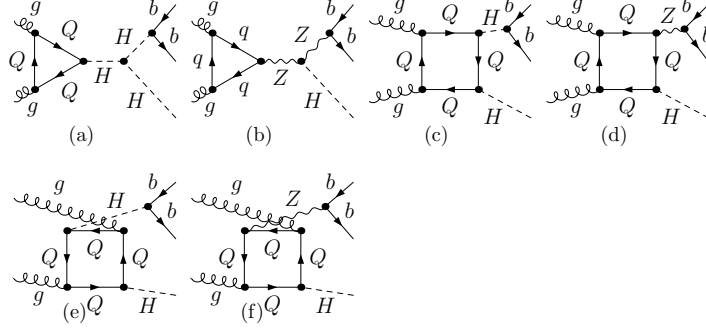


FIG. 3: The representative one-loop diagrams with possible resonance for the process $gg \rightarrow b\bar{b}H$. $Q = t, b$. $q = u, d, c, s, t, b$.

III. NUMERICAL STUDIES

A. Input parameters

For the numerical analysis we take the following input parameters [29],

$$\begin{aligned}
 G_\mu &= 1.1663787 \times 10^{-5} \text{ GeV}^{-2}, & M_W &= 80.385 \text{ GeV}, \\
 M_Z &= 91.1876 \text{ GeV}, & \Gamma_Z &= 2.4952 \text{ MeV}, \\
 M_t &= 173.1 \text{ GeV}, & M_H &= 125 \text{ GeV}.
 \end{aligned} \tag{4}$$

We adopt the MSTWlo2008 PDFs [30] with 4-flavor light quarks in the numerical analysis for NLO as well as LO predictions (since we are chiefly interested in assessing effects of matrix-element origin). If not otherwise specified, the renormalization scale and the factorization scale are set to be equal, that is, $\mu_R = \mu_F = (M_H + 2 \times m_b)/4$. As explained in section II B, the bottom quark mass is set as pole mass with 4.78 GeV. The decay width of Higgs boson is assumed to be $\Gamma_H = 6 \text{ MeV}$ [31].

Both the final state bottom and anti-bottom quarks is tagged by the following kinematic constraints:

$$p_T^{b/\bar{b}} > 30 \text{ GeV}, \quad |y^{b/\bar{b}}| < 2.5, \quad R_{b\bar{b}} > 0.4, \tag{5}$$

where $p_T^{b/\bar{b}}$ and $y^{b/\bar{b}}$ are the transverse momentum and rapidity of the bottom and anti-bottom quarks, respectively, and $R_{b\bar{b}}$ is the separation in the plane of azimuthal angle and rapidity between two b quarks.

B. Total cross sections

From the description in above section, we can obtain the total EW NLO corrected cross section for $pp \rightarrow b\bar{b}H$ process as

$$\sigma_{NLO}^{pp} = \sigma_{LO}^{pp} + \Delta\sigma_{EW}^{gg}, \quad (6)$$

where $\Delta\sigma_{EW}^{gg}$ is the summation of the virtual and real photon corrections for the subprocess $gg \rightarrow b\bar{b}H$.

We show the total LO and EW NLO cross section at the 13 TeV LHC in Table I for some typical values of the factorization/renormalization scale, where $\mu_R = \mu_F = \mu$ and $\mu_0 = (M_H + 2 \times m_b)/4$. The corresponding relative corrections δ in the last column are defined as $\delta = (\sigma_{NLO}^{pp} - \sigma_{LO}^{pp})/\sigma_{LO}^{pp}$. It's worth noting that, all the contributions of $q\bar{q}$ annihilations of the giving values of the factorization/renormalization scale are less 2% to the total cross section at LO. This is the very motivation that we only include the NLO EW correction of the gg subprocess. We can see that the EW NLO relative corrections don't vary with the factorization/renormalization scale, and the LO cross sections are suppressed by EW NLO corrections by about 4% at the 13 TeV LHC. To investigating the EW NLO contributions in variations of the bottom pole mass, we present the numerical results for typical values of bottom pole mass with upper value of 4.84 GeV, center value of 4.78 GeV and lower value 4.72 GeV [29] in Table II. We find that the EW NLO relative corrections remain the same with different bottom pole masses.

The integrated luminosity L of LHC will reach 300 fb^{-1} in its first 13-15 years of operation, then LHC will be substituted by the High Luminosity LHC (HL-LHC) with 3000 fb^{-1} [32]. The $b\bar{b}H$ associate production (with $H \rightarrow b\bar{b}$) at LHC has been proposed and systematically studied in [33]. The EW NLO corrections to the event number of $pp \rightarrow b\bar{b}H \rightarrow b\bar{b}b\bar{b}$ at the LHC/HL-LHC can be simply estimated by

$$\Delta N = (\sigma_{NLO}^{pp} - \sigma_{LO}^{pp}) \times Br(H \rightarrow b\bar{b}) \times L \times \epsilon_b^4, \quad (7)$$

where the branch ratio $Br(H \rightarrow b\bar{b}) = 58\%$ [31] and b-tagging efficiency $\epsilon_b = 77\%$ [34]. We can find that the EW NLO corrections reduce the event number by 48 at the 13 TeV LHC with 300 fb^{-1} for $\mu_R = \mu_F = \mu_0$, which can not be negligible roughly.

μ	$\sigma_{LO}^{gg} [\text{fb}]$	$\sigma_{LO}^{qq} [\text{fb}]$	$\sigma_{LO}^{pp} [\text{fb}]$	$\sigma_{NLO}^{pp} [\text{fb}]$	$\delta[\%]$
$\mu_0/4$	41.96(4)	0.6064(1)	42.57(4)	41.06(4)	-3.6
$\mu_0/2$	29.82(3)	0.4422(1)	30.26(3)	29.18(3)	-3.6
μ_0	21.62(2)	0.3354(1)	21.96(2)	21.18(2)	-3.6
$2\mu_0$	16.06(1)	0.26202(8)	16.32(1)	15.74(1)	-3.6
$4\mu_0$	12.21(1)	0.20949(6)	12.42(1)	11.97(1)	-3.6

TABLE I: The LO, NLO EW corrected integrated cross sections (σ_{LO} , σ_{NLO}) and the corresponding δ at the 13 TeV LHC for some typical values of the factorization/renormalization scale, where $\mu_R = \mu_F = \mu$ and $\mu_0 = (M_H + 2 \times m_b)/4$.

m_b (GeV)	$\sigma_{LO}^{gg} [\text{fb}]$	$\sigma_{LO}^{qq} [\text{fb}]$	$\sigma_{LO}^{pp} [\text{fb}]$	$\sigma_{NLO}^{pp} [\text{fb}]$	$\delta[\%]$
4.84	22.14(2)	0.3438(1)	22.49(2)	21.69(2)	-3.6
4.78	21.62(2)	0.3354(1)	21.96(2)	21.18(2)	-3.6
4.72	21.11(2)	0.3271(1)	21.44(2)	20.67(2)	-3.6

TABLE II: The LO, NLO EW corrected integrated cross sections (σ_{LO} , σ_{NLO}) and the corresponding δ at the 13 TeV LHC with different bottom pole mass.

C. Differential cross sections

In the following, we turn to the differential distributions of various kinematic variables at the 13 TeV LHC. The relative NLO EW corrections to the differential cross section $d\sigma/dx$ are defined as $\delta(x) = \left(\frac{d\sigma_{NLO}}{dx} - \frac{\sigma_{LO}}{dx} \right) / \frac{\sigma_{LO}}{dx}$, where x stands for kinematic observable, i.e., the transverse momentum of the bottom quark (p_T^b) and the Higgs boson (p_T^H), the invariant mass of $b\bar{b}$ pair ($M_{b\bar{b}}$) and the separation between two bottom quarks ($R_{b\bar{b}}$) in this paper.

In Fig.4(a) and (b), we depict the LO and NLO EW corrected distributions for the transverse momentum of the final state bottom or anti-bottom quark with highest (leading) and second highest (sub-leading) p_T and the Higgs boson. The leading (sub-leading) b-jet is labelled by $b_1(b_2)$ and colored red (blue). The Fig.5(a) and (b) present the LO and NLO EW corrected distributions of $M_{b\bar{b}}$ and $R_{b\bar{b}}$ separately. The corresponding relative NLO EW corrections are also shown. We can see that all the LO distributions of the considered observables (except $p_T^{b_2}$) are suppressed by the EW corrections in the plotted region. It can be also seen that the EW corrections don't vary the shape of the LO distributions. For the transverse momentum of the leading and sub-leading b-jets, the LO and EW corrected distributions both always decrease with the increment of p_T^b and the

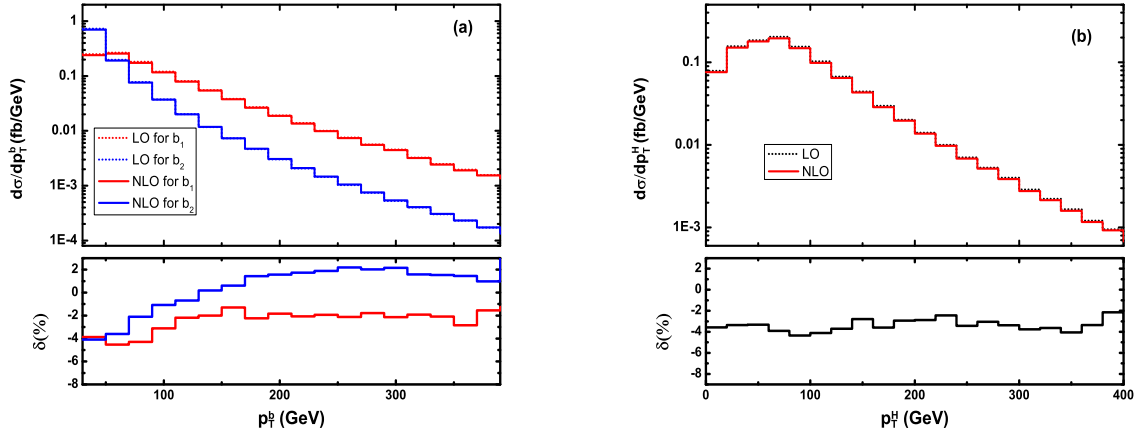


FIG. 4: The LO, NLO EW corrected distributions and the relative NLO EW corrections of $pp \rightarrow b\bar{b}H + X$ process at the 13 TeV LHC for p_T^b (a) and p_T^H (b).

relative EW corrections can be about -4.5% (-4.1%) in the low $p_T^{b_1}$ ($p_T^{b_2}$) region. For the transverse momentum of the Higgs boson, all the LO and EW corrected distributions reach maximum when $p_T^H \sim 60$ GeV and the corresponding relative EW corrections can mount to about -3.9% . From the curve of relative EW corrections of the invariant mass of the bottom quark pair, we can find an obvious oscillation. This oscillation shows the singular pole structure we mentioned in II B: as the invariant mass of bottom quark pair approaches the Higgs boson mass or the Z boson mass, there exist resonant propagators in the virtual diagrams, which lead the oscillation in the invariant mass distributions. All the LO and EW corrected distributions of $R_{b\bar{b}}$ have peak when $R_{b\bar{b}} \sim 3$, and the values of relative EW corrections do not vary too much and almost lie in the range of $[-3\% \sim -5\%]$ in the plotted region.

IV. SUMMARY

In this work we have analysed the EW effects for the Higgs boson production associated with two bottom quarks at the LHC. From the numerical analysis, we noticed that at LO (i.e., $\alpha_s^2\alpha$) the gg channel is the dominant contribution compared with the other subprocesses initiated by quark pair. Based on the fact of this observation, we only include the EW NLO corrections for the gg channel. We present the calculation with some typical values of the factorization/renormalization scale and bottom pole mass, and find that the EW NLO relative corrections are all -3.6% . We also investigate the various kinematic distributions of the final state particles, the bottom and

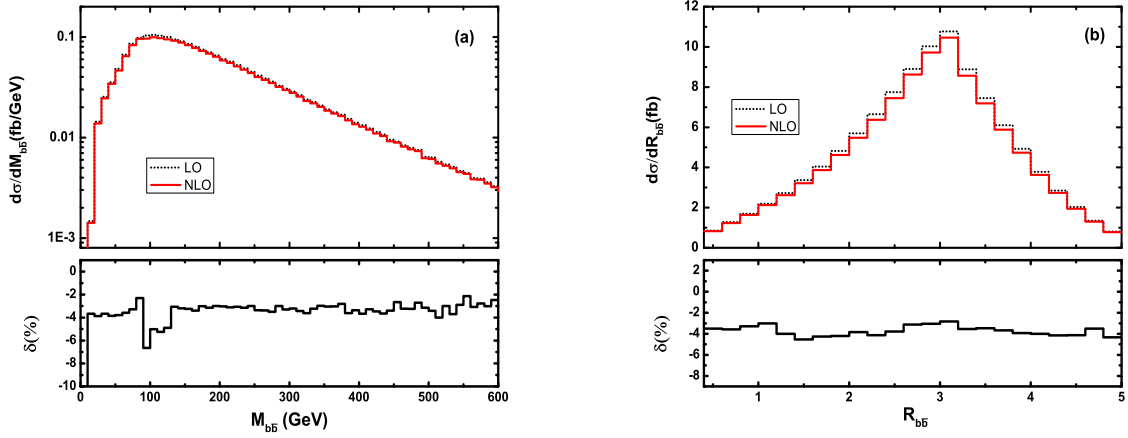


FIG. 5: The LO, NLO EW corrected distributions and the relative NLO EW corrections of $pp \rightarrow b\bar{b}H + X$ process at the 13 TeV LHC for $M_{b\bar{b}}$ (a) and $R_{b\bar{b}}$ (b).

anti-bottom quarks and the Higgs boson and find that NLO EW corrections are always negative except in some regions of $p_T^{b_2}$.

Acknowledgements

This work was supported by the China Postdoctoral Science Foundation (Grant No.2017M611771).

-
- [1] G. Aad *et al.* [ATLAS Collaboration], Phys. Lett. B **716**, 1 (2012) [arXiv:1207.7214 [hep-ex]].
 - [2] S. Chatrchyan *et al.* [CMS Collaboration], Phys. Lett. B **716**, 30 (2012) [arXiv:1207.7235 [hep-ex]].
 - [3] **ATLAS Collaboration**, G. Aad *et al.*, *Combined coupling measurements of the Higgs-like boson with the ATLAS detector using up to 25 fb⁻¹ of proton-proton collision data*, ATLAS-CONF-2013-034, ATLAS-COM-CONF-2013-035.
 - [4] **CMS Collaboration**, S. Chatrchyan *et al.*, *Observation of a new boson with mass near 125 GeV in pp collisions at $\sqrt{s} = 7$ and 8 TeV*, JHEP **1306** (2013) 081, [arXiv:1303.4571].
 - [5] J. M. Campbell *et al.*, hep-ph/0405302.
 - [6] D. Dicus, T. Stelzer, Z. Sullivan and S. Willenbrock, Phys. Rev. D **59** (1999) 094016 doi:10.1103/PhysRevD.59.094016 [hep-ph/9811492].
 - [7] C. Balazs, H. J. He and C. P. Yuan, Phys. Rev. D **60** (1999) 114001 doi:10.1103/PhysRevD.60.114001 [hep-ph/9812263].

- [8] R. V. Harlander and W. B. Kilgore, Phys. Rev. D **68** (2003) 013001 doi:10.1103/PhysRevD.68.013001 [hep-ph/0304035].
- [9] S. Dittmaier, M. Kramer, I. A. Muck and T. Schluter, JHEP **0703** (2007) 114 doi:10.1088/1126-6708/2007/03/114 [hep-ph/0611353].
- [10] J. M. Campbell, R. K. Ellis, F. Maltoni and S. Willenbrock, Phys. Rev. D **67** (2003) 095002 doi:10.1103/PhysRevD.67.095002 [hep-ph/0204093].
- [11] S. Dawson, C. B. Jackson, L. Reina and D. Wackeroth, Phys. Rev. Lett. **94** (2005) 031802 doi:10.1103/PhysRevLett.94.031802 [hep-ph/0408077].
- [12] S. Dawson and C. B. Jackson, Phys. Rev. D **77** (2008) 015019 doi:10.1103/PhysRevD.77.015019 [arXiv:0709.4519 [hep-ph]].
- [13] S. Dawson and P. Jaiswal, Phys. Rev. D **81** (2010) 073008 doi:10.1103/PhysRevD.81.073008 [arXiv:1002.2672 [hep-ph]].
- [14] M. Beccaria, G. O. Davier, G. Macorini, E. Mirabella, L. Panizzi, F. M. Renard and C. Verzegnassi, Phys. Rev. D **82** (2010) 093018 doi:10.1103/PhysRevD.82.093018 [arXiv:1005.0759 [hep-ph]].
- [15] S. Dittmaier, M. Krmer and M. Spira, Phys. Rev. D **70** (2004) 074010 doi:10.1103/PhysRevD.70.074010 [hep-ph/0309204].
- [16] S. Dawson, C. B. Jackson, L. Reina and D. Wackeroth, Phys. Rev. D **69** (2004) 074027 doi:10.1103/PhysRevD.69.074027 [hep-ph/0311067].
- [17] S. Dawson, C. B. Jackson, L. Reina and D. Wackeroth, Mod. Phys. Lett. A **21** (2006) 89 doi:10.1142/S0217732306019256 [hep-ph/0508293].
- [18] M. Wiesemann, R. Frederix, S. Frixione, V. Hirschi, F. Maltoni and P. Torrielli, JHEP **1502**, 132 (2015) [arXiv:1409.5301 [hep-ph]].
- [19] A. Denner, Fortsch. Phys. **41**, 307 (1993) [arXiv:0709.1075 [hep-ph]].
- [20] N. Baro, F. Boudjema and A. Semenov, Phys. Rev. D **78** (2008) 115003 doi:10.1103/PhysRevD.78.115003 [arXiv:0807.4668 [hep-ph]].
- [21] D. T. Nhung, W. Hollik and L. D. Ninh, Phys. Rev. D **87**, no. 11, 113006 (2013) [arXiv:1210.4087 [hep-ph]].
- [22] B. W. Harris and J. F. Owens, Phys. Rev. D **65** (2002) 094032 doi:10.1103/PhysRevD.65.094032 [hep-ph/0102128].
- [23] S. Catani and M. H. Seymour, Phys. Lett. B **378** (1996) 287 doi:10.1016/0370-2693(96)00425-X [hep-ph/9602277].
- [24] S. Catani and M. H. Seymour, Nucl. Phys. B **485** (1997) 291 Erratum: [Nucl. Phys. B **510** (1998) 503] doi:10.1016/S0550-3213(96)00589-5, 10.1016/S0550-3213(98)81022-5 [hep-ph/9605323].
- [25] S. Catani, S. Dittmaier, M. H. Seymour and Z. Trocsanyi, Nucl. Phys. B **627** (2002) 189 doi:10.1016/S0550-3213(02)00098-6 [hep-ph/0201036].
- [26] T. Hahn, Comput. Phys. Commun. **140** (2001) 418 doi:10.1016/S0010-4655(01)00290-9 [hep-ph/0012260].

- [27] T. Hahn and M. Perez-Victoria, Comput. Phys. Commun. **118** (1999) 153 doi:10.1016/S0010-4655(98)00173-8 [hep-ph/9807565].
- [28] A. Denner and S. Dittmaier, Nucl. Phys. B **658** (2003) 175 doi:10.1016/S0550-3213(03)00184-6 [hep-ph/0212259].
- [29] C. Patrignani *et al.* [Particle Data Group], Chin. Phys. C **40** (2016) no.10, 100001. doi:10.1088/1674-1137/40/10/100001
- [30] A. D. Martin, W. J. Stirling, R. S. Thorne and G. Watt, Eur. Phys. J. C **63** (2009) 189 doi:10.1140/epjc/s10052-009-1072-5 [arXiv:0901.0002 [hep-ph]].
- [31] V. Barger, M. Ishida and W. Y. Keung, Phys. Rev. Lett. **108**, 261801 (2012) [arXiv:1203.3456 [hep-ph]].
- [32] G. Apollinari, O. Brning, T. Nakamoto and L. Rossi, CERN Yellow Report (2015) no.5, 1 doi:10.5170/CERN-2015-005.1 [arXiv:1705.08830 [physics.acc-ph]].
- [33] C. Balazs, J. L. Diaz-Cruz, H. J. He, T. M. P. Tait and C. P. Yuan, Phys. Rev. D **59** (1999) 055016 doi:10.1103/PhysRevD.59.055016 [hep-ph/9807349].
- [34] ATLAS Collaboration, Optimisation of the ATLAS b-tagging performance for the 2016 LHC Run, ATL-PHYS-PUB-2016-012, 2016, url:<https://cds.cern.ch/record/2160731>.